

Efficient EMD and Hilbert spectra computation for 3D geometry processing and analysis via space-filling curve

Xiaochao Wang¹ · Jianping Hu² · Dongbo Zhang¹ · Hong Qin³

Published online: 25 April 2015
© Springer-Verlag Berlin Heidelberg 2015

Abstract Empirical Mode Decomposition (EMD) has proved to be an effective and powerful analytical tool for non-stationary time series and starts to exhibit its modeling potential for 3D geometry analysis. Yet, existing EMD-based geometry processing algorithms only concentrate on multi-scale data decomposition by way of computing intrinsic mode functions. More in-depth analytical properties, such as Hilbert spectra, are hard to study for 3D surface signals due to the lack of theoretical and algorithmic tools. This has hindered much more broader penetration of EMD-centric algorithms into various new applications on 3D surface. To tackle this challenge, in this paper we propose a novel and efficient EMD and Hilbert spectra computational scheme for 3D geometry processing and analysis. At the core of our scheme is the strategy of dimensionality reduction via space-filling curve. This strategy transforms the problem of 3D geometry analysis to 1D time series processing, leading to two major advantages. First, the envelope computation is carried out for 1D signal by cubic spline interpolation, which is much faster than existing envelope computation directly over

3D surface. Second, it enables us to calculate Hilbert spectra directly on 3D surface. We could take advantages of Hilbert spectra that contain a wealth of unexploited properties and utilize them as a viable indicator to guide our EMD-based 3D surface processing. Furthermore, to preserve sharp features, we develop a divide-and-conquer scheme of EMD by explicitly separating the feature signals from non-feature signals. Extensive experiments have been carried out to demonstrate that our new EMD and Hilbert spectra based method is both fast and powerful for 3D surface processing and analysis.

Keywords Empirical mode decomposition · Hilbert spectra · Space-filling curve · Surface processing

1 Introduction

Empirical mode decomposition (EMD) has been gradually gaining popularity with increasing interest ever since its inception into signal processing by Huang et al. [13]. EMD is initially designed for 1D signal processing and has proved to be a powerful tool for non-stationary and non-linear time series. Drastically different from conventional signal processing technologies (e.g., Fourier and wavelet analysis), which project a signal onto the pre-specified basis functions, EMD decomposes a signal to a sum of intrinsic mode functions (IMFs) and a monotonic residue. Such IMFs are empirical in nature, and are signal-dependent and data-adaptive. Directly benefitting from these adaptive basis functions, EMD is thoroughly data-driven and performs well for non-linear and non-stationary signal analysis.

There have been a plethora of EMD-based methods in 1D signal [6, 13, 15, 16], and 2D image processing [2, 23, 33], yet EMD algorithms on manifold for 3D geometry analysis and processing are rare and their overall growth is still in their

✉ Jianping Hu
neduhjp307@163.com

Xiaochao Wang
wangxiaochao18@gmail.com

Dongbo Zhang
zhangdongbo9212@163.com

Hong Qin
qin@cs.stonybrook.edu

¹ State Key Laboratory of Virtual Reality Technology and Systems, Beihang University, Beijing 100191, China

² College of Sciences, Northeast Dianli University, Jilin 132012, China

³ Department of Computer Science, Stony Brook University, Stony Brook, NY 11794-4400, USA

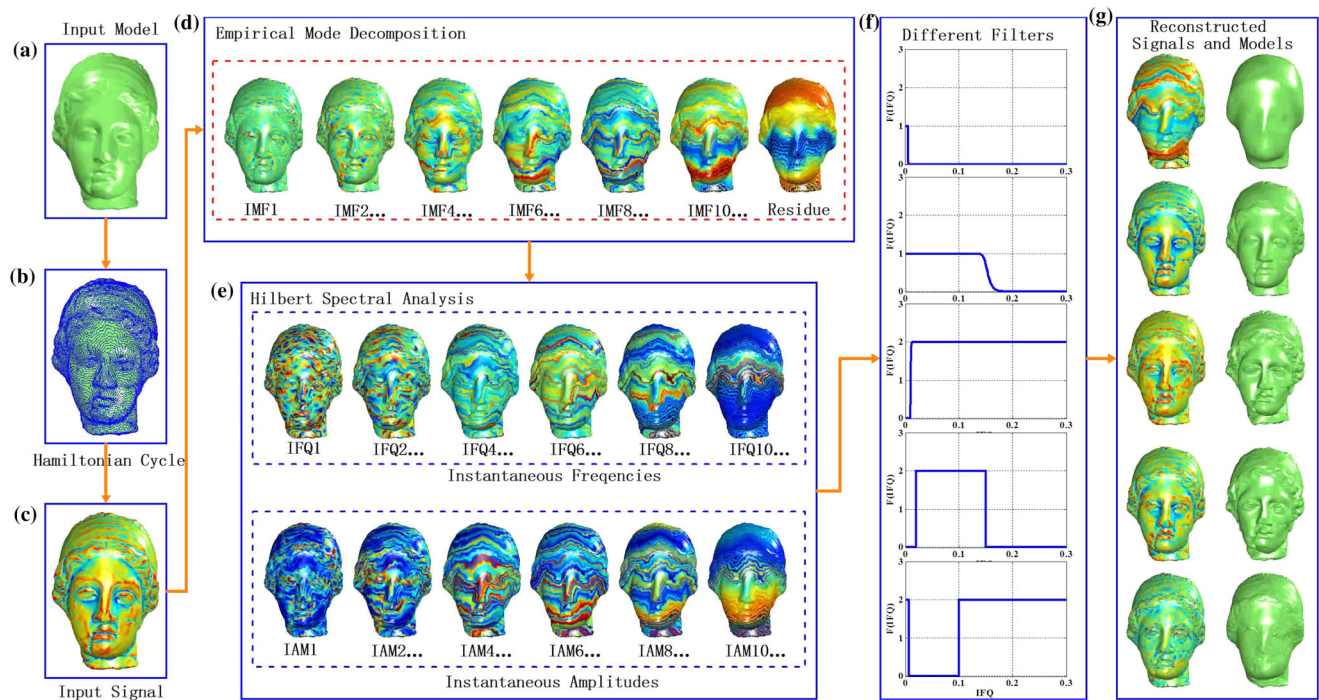


Fig. 1 Pipeline of EMD and Hilbert spectra computation for 3D geometry processing and analysis. **a** Input model. **b** One type of space-filling curve (Hamiltonian cycle) traversing the model. **c** Geometry signal based on the mean curvature. **d** EMD with the obtained IMFs and

residue. **e** Hilbert spectral analysis on IMFs, where instantaneous frequencies (IFQs) and Instantaneous amplitudes (IAMs) are computed. **f** Different filter designs for IFQs. **g** Modified signals and geometric reconstruction

infancy, full potential of EMD for manifold are not realized. Until now, fewer work on EMD for 3D surface has been reported [12, 18, 26]. One main challenge of extending the original EMD to 3D surface is how to calculate the envelopes of the data in an effective way. The existing envelope computing algorithms directly generalize the 1D EMD to surfaces and work well for small-sized models. Nonetheless, existing algorithms remain to be extremely time-consuming for large-sized models.

Besides suffering from being ineffective for the existing methods, the Hilbert spectra can not be directly computed on 3D surface due to the lack of theoretical and algorithmic tools. This limitation also prevents more broader propagation of EMD-centric algorithms into many urgently-needed applications over 3D surface. To resolve these problems, we propose an efficient EMD and Hilbert spectra computational scheme for 3D surface analysis and processing via space-filling curve, inspired by the idea of dimensionality reduction [8, 20]. This strategy transforms the problem of EMD-centric 3D surface processing into 1D time series processing. It is fully taking advantage of original 1D EMD and greatly improves the computational performance. The pipeline of EMD and Hilbert spectra analysis¹ is shown in

¹ The process of EMD and Hilbert spectra analysis is called Hilbert-Huang transform (HHT) in the literature.

Fig. 1. Moreover, to overcome the feature-blurring effects of EMD and preserve potential sharp features in 3D surface, we develop a divide-and-conquer scheme of EMD by explicitly separating the feature signals from non-feature signals.

The key contributions of our work can be summarized as follows:

- The problem of EMD-centric 3D surface processing is converted to 1D EMD signal processing by adopting the dimensionality reduction via space-filling curve. Fully taking advantage of 1D original EMD, the proposed EMD-centric 3D surface analysis and processing algorithm is significantly accelerated.
- Different from existing EMD-based works on 3D surface, which only focus on multi-scale data decomposition, we are capable of computing the Hilbert spectra, and more properties of Hilbert spectra are exploited for 3D surface analysis and processing.
- By distinguishing the features from non-features and arranging them into several feature segments, we develop a divide-and-conquer EMD decomposition scheme, which explicitly preserves the global/local feature structures in a piecewise manner and overcomes the feature-blurring effects of traditional EMD.

2 Related work

We now briefly review the related work of EMD, signal processing on 3D surface, and space-filling curves.

Empirical mode decomposition. In 1998, Huang et al. [13] proposed an EMD method for 1D signal processing and analysis, which is data-driven and especially for non-linear and non-stationary signals. It uses a sifting process to generate IMFs, which represent different scale oscillatory modes of the given signal. This method overcomes the limitation of traditional time-frequency analysis methods (e.g., Fourier and wavelet analysis) that depend on the pre-defined basis functions and has been applied to various 1D signal processing.

EMD has also been extended directly to analyze high-dimensional signals [8,20,31]. The critical step of this extension is the interpolation from extremum at each iteration in high-dimension, which makes the EMD process complicated and time-consuming. In order to improve the efficiency, Gao et al. [8] and Ren et al. [20] adopted space-filling curve to *flatten* 3D data into 1D data to reduce the computational cost in flow field simulation. These algorithms are typically applied on 2D or 3D regular grids. However, unlike the regular domains in Euclidean space, 3D surfaces are irregular, curved, and possibly have any complex structures, which will give rise to more challenges for fast EMD computation.

Signal processing on 3D surface. Fourier transform is a classical signal processing and analysis tool and can be directly adapted onto manifold. It can represent shape as superposition of Laplace-Beltrami eigenfunctions analogous to sines and cosines of the Fourier transform in the Euclidean space. This characteristic is first used by Taubin [24] to develop a signal processing framework for mesh fairing.

Different from Fourier transform, wavelet transform is a more powerful tool for signal processing because of its locality in both time/space and frequency domains. At present, subdivision wavelets [10], spherical wavelets [21], diffusion wavelets [5,11,28] and graph wavelets [36] have been proposed for 3D surface, which can benefit various applications, e.g., mesh compression, visualization, and retrieval.

As a novel fully adaptive and data-driven time frequency analysis method, EMD has gained great success in 1D and 2D data processing. Motivated by such success, it has also been used for 3D surface processing [12,18,26]. The earlier method [18] based on 2D interpolation and mesh parameterizations technology prevents its further application to topologically more complex surface. An alternative based on bi-harmonic interpolation [12,26] is extremely time-consuming for large-sized models. To overcome these limitations, we present an efficient EMD and Hilbert spectra computation for 3D surface analysis and processing via space-filling curve.

Space-filling curve on 3D surface. Space-filling curve is a continuous curve passing through every point of the unit square, which is first discovered by Peano [17]. In literatures, different types of space-filling curve have been proposed, such as Z-curve, Hilbert curve, Gosper curve, and Koch curve. Most of the space-filling curve generation algorithms are applied on 2D or 3D regular grids, fewer algorithms are proposed for generating space-filling curve on irregular and complex 3D surfaces [19]. However, the method of [19] heavily relies on mesh parametrization and treats each patch's curve independently without connecting them to form one complete curve.

Without restoring to mesh parametrization, another compact connectivity representation (called Hamiltonian cycle) on 3D surface can be viewed as a new space-filling curve. To generate the Hamiltonian cycle on 3D surface, Taubin [25] showed that Hamiltonian cycle can be always generated from the connected manifold quadrilateral mesh without boundary. Following this observation, Ergun et al. [1] first converted the triangular mesh into quadrilateral mesh, then generated the Hamiltonian cycle by adopting Taubin's algorithm [25]. It is cumbersome to convert the triangular mesh to quadrilateral mesh, which not only changes the original geometry structure, but also is time-consuming. In this paper, an effective yet approximate Hamiltonian cycle generation algorithm proposed by Gurung et al. [9] is adopted, which can fully meet our requirements.

3 Hamiltonian cycle and 1D EMD

In this section, we will describe Hamiltonian cycle generation, the processes of EMD and Hilbert transform.

3.1 Hamiltonian cycle on 3D surface

Given a 3D surface \mathbf{S} , which can be discretized into a triangular mesh $\mathbf{M} = (\mathbf{V}, \mathbf{F})$. \mathbf{V} denotes the set of vertices with geometry coordinates $\mathbf{v}_i = (x_i, y_i, z_i) \in R^3, i = 1, \dots, n$, and $\mathbf{f}_j = (\mathbf{v}_{j1}, \mathbf{v}_{j2}, \mathbf{v}_{j3}), j = 1, \dots, m$ is a primitive array containing the indices of vertices for defining triangle faces. In graph theory, the problem of Hamiltonian cycle is to find a cycle passing through every vertex exactly once on a given graph. For triangular mesh, Hamiltonian cycle is a closed curve visiting vertices of the mesh once and only once and has been widely used in triangular mesh processing, such as model rendering [3], mesh compression [34], shape sculpture [1]. For generating Hamiltonian cycle on 3D surface, a greedy RING-EXPANDER algorithm [9] is adopted here, which is simple and linear in time and space. Figure 2 shows an example about the generated Hamiltonian cycle on a triangular mesh.

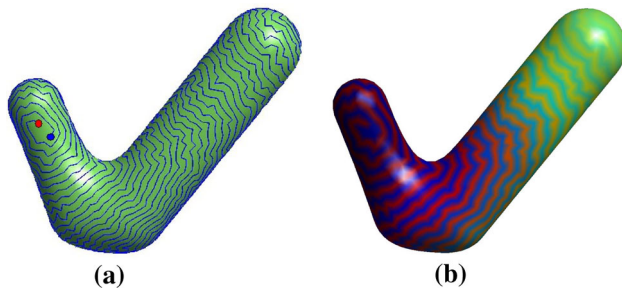


Fig. 2 An example about the generated Hamiltonian cycle. **a** Hamiltonian cycle is shown in *blue line* with the starting and ending points marked in *blue* and *red* colors, respectively. **b** The mesh is *color-coded* from *blue* to *red* in ring order

Hamiltonian cycle contains more than 99.99% of the vertices [9] and leaves fewer isolated vertices unvisited. The values of these isolated vertices can be easily interpolated by the values of its one-ring neighbors. Therefore, for convenience, we assume that there are no isolated vertices in following process.

3.2 1D EMD for signal processing

Hamiltonian cycle converts the problem of 3D signal processing into 1D signal processing, which can be effectively dealt with by 1D EMD. The central idea of EMD is to decompose a signal by a sifting process into several IMFs and a residue, which represent the fine-scale details and a trend of signal. A signal to be a IMF should satisfies the two following conditions [13]:

- First, in the whole data set, the number of extreme and the number of zero crossing must equal or differ at most by one;
- Second, at any point, the mean value of the envelope defined by the local maxima and the envelope defined by the local minima is zero.

Specifically, for a given signal $\mathbf{G}(t)$, $t \in \mathbf{R}^1$, the process of EMD is summarized in Algorithm 1. Through the EMD algorithm, the input signal \mathbf{G} can be represented by

$$\mathbf{G} = \sum_{k=1}^K \mathbf{h}_k + \mathbf{r}_K, \quad (1)$$

where \mathbf{h}_k are IMFs of \mathbf{G} and \mathbf{r}_K is the residue.

Stopping criteria of sifting process. To guarantee a signal could be decomposed into meaningful IMFs, a criterion needs to be set to stop the sifting processing, which can be achieved by restricting the size of the standard deviation

$$SD = \sum_{t=1}^n \frac{|s_{i-1}(t) - s_i(t)|^2}{|s_{i-1}(t)|^2}, \quad (2)$$

Algorithm 1 EMD Algorithm on 1D Signal

Input: 1D original signal $\mathbf{G}(t)$
Output: IMFs \mathbf{h}_k , $k = 1, \dots, K$ and a residue \mathbf{r}_K
Initialization: Set the first index of IMFs $k = 1$ and initial residue $\mathbf{r}_0 = \mathbf{G}$;
1: repeat
2: $\mathbf{s}_0 = \mathbf{r}_{k-1}$, $i = 1$;
3: for each i do
4:Find all local minima and local maxima of \mathbf{s}_{i-1} ;
5:Built the lower envelope \mathbf{LE}_{i-1} and upper envelope \mathbf{UE}_{i-1} by interpolating all local minima and maxima using cube spline, respectively;
6:Compute the mean envelope \mathbf{ME}_{i-1} of \mathbf{s}_{i-1} by $\mathbf{ME}_{i-1} = (\mathbf{LE}_{i-1} + \mathbf{UE}_{i-1})/2$;
7: $\mathbf{s}_i = \mathbf{s}_{i-1} - \mathbf{ME}_{i-1}$;
8: if \mathbf{s}_i satisfies the stopping criterion **then**
9:Get the $k - th$ IMF $\mathbf{h}_k = \mathbf{s}_i$ and the $k - th$ residue $\mathbf{r}_k = \mathbf{r}_{k-1} - \mathbf{h}_k$;
10: $k = k + 1$;
11: break;
12: else
13: $i = i + 1$;
14: end if
15: end for
16: until The residue is a constant or monotonic function

where \mathbf{s}_{i-1} and \mathbf{s}_i are two consecutive sifting functions in one iteration. The smaller the value is, the more IMFs we will get. In this paper, the default value of SD is 0.1.

Stopping criteria of EMD. Different from previous algorithms [12, 26], we expect a signal can be fully decomposed, which will give us more flexibility to manipulate the signal. So, the maximum number of IMFs is not limited. On the other hand, due to the large size of the mesh or signal, there will be so many generated IMFs. In order to explore a tradeoff between the efficiency of the algorithm and the complete signal decomposition, the whole EMD will be stopped if either the number of maximum or minimum of the residue are smaller than a presetting value, and this pre-defined value is set to be 15 in all our experiments.

3.3 Hilbert transform and Hilbert spectra

After decomposing a signal into a number of IMFs and a residue, the Hilbert transform can be applied to each IMF and the instantaneous frequency as well as instantaneous amplitude can be calculated.

For any given signal $\mathbf{q}(t)$, $t \in \mathbf{R}^1$, the Hilbert transform is defined as

$$\mathbf{Q}(t) = \frac{1}{\pi} P \int_{-\infty}^{+\infty} \frac{\mathbf{q}(t')}{t - t'} dt', \quad (3)$$

where P indicates the Cauchy principal value [13]. Following the definition, $\mathbf{q}(t)$ and $\mathbf{Q}(t)$ comprise the complex conjugate pair and form an analytic signal, $\mathbf{I}(t)$,

$$\mathbf{I}(t) = \mathbf{q}(t) + \mathbf{i}\mathbf{Q}(t) = a(t)e^{i\theta(t)}, \tag{4}$$

where \mathbf{i} is the imaginary unit, $\theta(t)$ and $a(t)$ are the instantaneous phase and instantaneous amplitude, which are computed by

$$a(t) = \sqrt{\mathbf{q}^2(t) + \mathbf{Q}^2(t)}, \tag{5}$$

and

$$\theta(t) = \arctan\left(\frac{\mathbf{Q}(t)}{\mathbf{q}(t)}\right). \tag{6}$$

Furthermore, based on the instantaneous phase, the instantaneous frequency can be defined as

$$\omega = \frac{d\theta(t)}{dt}, \tag{7}$$

once the Hilbert transform has been applied to each IMF, the signal $\mathbf{G}(t)$ can be expressed by

$$\mathbf{G}(t) = Re\left(\sum_{i=1}^K a_i(t) \exp\left(\mathbf{i} \int_{-\infty}^{+\infty} \omega_i(t) dt\right)\right) + \mathbf{r}_K, \tag{8}$$

where Re is the operator of real-part operator. The steps of Hilbert spectra computation on 3D surface are presented in Algorithm 2 and the computed Hilbert spectra of Igea are shown in Fig. 1e.

Algorithm 2 Hilbert Spectra Computation on 3D Surface

Input: All IMFs $\mathbf{h}_k, k = 1, \dots, K$
Output: Hilbert spectra (including the instantaneous amplitude, phase, and frequency)
 1: **for** each k **do**
 2: Compute the Hilbert transform of \mathbf{h}_k by Eq. 3;
 3: Compute the amplitude of \mathbf{h}_k by Eq. 5;
 4: Compute the phase of \mathbf{h}_k by Eq. 6;
 5: Compute the instantaneous frequency of \mathbf{h}_k by Eq. 7;
 6: **end for**

4 Signal processing guided by Hilbert spectra

In this section, we will first define a signal on the input model and then develop an adaptive signal processing framework guided by Hilbert spectra.

4.1 Signal definition and reconstruction

To effectively deal with 3D surface based on EMD and Hilbert spectra, signal should be careful defined first. In this paper, the signal $\mathbf{G}(\mathbf{v}_i)$ of mean curvatures used in [12] is adopted, which is rotation-invariant, translation-invariant and

facilitates the computation of multi-scale features of surface. The signal $\mathbf{G}(\mathbf{v}_i)$ is defined on vertices of 3D surface and can be transformed into 1D signal $\mathbf{G}(t)$ according to the order of vertex appearing in Hamiltonian cycle.

Surface reconstruction. To reconstruct the new mesh with vertex positions $\tilde{\mathbf{V}}$ from the modified signal $\tilde{\mathbf{G}}$, we adopt a mesh reconstruction algorithm under Laplacian framework by minimizing the energy with constraint of original vertex

$$\|\mathbf{L}\tilde{\mathbf{V}} - \text{diag}(\tilde{\mathbf{G}})\mathbf{N}\|^2 + \lambda^2 \sum_{i=1}^n \|\tilde{\mathbf{v}}_i - \mathbf{v}_i\|^2, \tag{9}$$

where λ is a weight of original vertex position, the default value is 0.01. $\text{diag}(\tilde{\mathbf{G}})$ returns a square diagonal matrix with the elements of vector $\tilde{\mathbf{G}}$ on the main diagonal. \mathbf{N} is the vertex normal matrix and \mathbf{L} is the Laplacian matrix with elements of

$$\mathbf{L}_{ij} = \begin{cases} \sum_{j \in N(i)} w_{ij}, & \text{if } i = j \\ -w_{ij}, & \text{if } j \in N(i), \\ 0, & \text{otherwise} \end{cases} \tag{10}$$

where $N(i)$ is the vertex set of the 1-ring neighbors of \mathbf{v}_i . w_{ij} is weight defined by $w_{ij} = (\cot \alpha_{ij} + \cot \beta_{ij})/2\mathcal{A}_i$. $\cot \alpha_{ij}$ and $\cot \beta_{ij}$ are the angles opposite to the edge (i, j) and \mathcal{A}_i is the Voronoi area of vertex \mathbf{v}_i .

Rewrite the energy of Eq. 9 into a linear system

$$\begin{bmatrix} \mathbf{L} \\ \lambda \mathbf{I}_{n \times n} \end{bmatrix} \tilde{\mathbf{V}} = \begin{bmatrix} \text{diag}(\tilde{\mathbf{G}})\mathbf{N} \\ \lambda \mathbf{V} \end{bmatrix}, \tag{11}$$

which can be efficiently solved in the least-squares sense with $\mathbf{A}^T \mathbf{A} \tilde{\mathbf{V}} = \mathbf{A}^T \mathbf{b}$ by Cholesky factorization.

4.2 Hilbert spectra-based surface processing

The computed instantaneous frequency explicitly gives the frequency distribution of multi-scale IMFs and enables us to filter the specified frequency of signal directly. Therefore, Hilbert spectra-based signal processing framework is defined as

$$\begin{aligned} \tilde{\mathbf{G}}(t) &= Re\left(\sum_{i=1}^K \tilde{a}_i(t) \cdot \exp\left(\mathbf{i} \int_{-\infty}^{+\infty} \omega_i(t) dt\right)\right) + \mathbf{r}_K \\ &= \sum_{i=1}^K \tilde{a}_i(t) \cdot \cos(\theta(t)) + \mathbf{r}_K, \end{aligned} \tag{12}$$

where $\tilde{a}_i(t)$ is the modified instantaneous amplitude by filtering the specific frequency signal.

Frequency distribution of the Hygeia model is shown in Fig. 3, which provides more intuitive information for signal

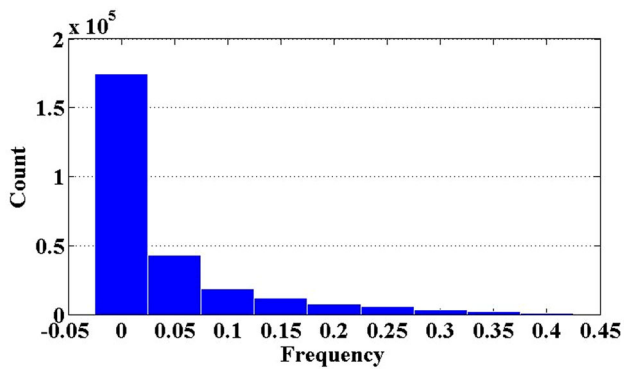


Fig. 3 Distribution of frequencies of Hygeia model, which is shown in Fig. 1

filtering. Therefore, different filters can be applied on instantaneous frequency $\omega_i(t)$, such as the low-pass, high-pass, band-pass and band-stop filters, to arrive at various results, which can be illustrated from the reconstructed signals and results shown in Fig. 1g.

After performing filters on $\omega_i(t)$, the modified instantaneous amplitude $\tilde{a}_i(t)$ can be obtained by

$$\tilde{a}_i(t) = \varphi(\omega_i(t)) \cdot a_i(t), \quad (13)$$

and the final modified signal is further expressed by

$$\tilde{\mathbf{G}}(t) = \sum_{i=1}^K \varphi(\omega_i(t)) \cdot a_i(t) \cdot \cos(\theta(t)) + \mathbf{r}_K, \quad (14)$$

Hilbert spectra transforms the problem of 3D surface processing from the spatial domain to frequency domain, which is much more straightforward than previous EMD-based surface processing methods, and the instantaneous frequency affords intuitive clue to guide the signal processing.

4.3 Feature-preserved surface smoothing

In the literature, there are many algorithms are proposed to preserve features during surface smoothing [7, 14, 22, 27].

However, the original EMD is not feature-aware, it could not preserve sharp features during the processing. To overcome this limitation, we propose an effective divide-and-conquer scheme, in which the feature vertices are treated separately from non-feature vertices.

At the beginning, the sharp features should be extracted first. In this work, a feature detection algorithm based on neighbor supporting [29] is adopted. The detected feature vertices are typically not isolated and can be further linked into several feature lines, and result in different feature signals. Figure 4c, d shows the extracted feature vertices in red color and the connected feature lines in distinct colors.

Then, these feature signals are processed independently using the proposed algorithm in the above section. For feature processing, there are two cases requiring special treatments. First, if there are corners detected from the model, the signals of these corners are averaged among the same type of corners. Second, if the length of a feature line is smaller than the predefined number of extremes reserved in the residue, the EMD would not be operated. These short feature signals should be processed in a reasonable manner. For instance, the Laplace smoothing or Bilateral filtering can be applied on these short signals if smoothing or denoising are needed.

To separate the feature signal from original signal, in each iteration of sifting process, the indices of features are always removed from the indices of the detected local extremum. Then the envelopes are computed by interpolating the remaining local extremum. That is, the feature signals do not participate in non-feature signals decomposition and the influence between them can be reduced as much as possible. After separating and decomposing the feature signals and non-feature signals by 1D EMD, they will be processed individually to obtain the new signals by our proposed Hilbert spectra based method. Finally, the modified feature signals and the non-feature signals are re-combined to reconstruct the new model.

Figure 4b, e shows the original signal and the processed signal of a noisy cube, respectively. From the result, we can see that after performing our algorithm, the sharp feature signals are shown in clear way with the noisy signals effectively

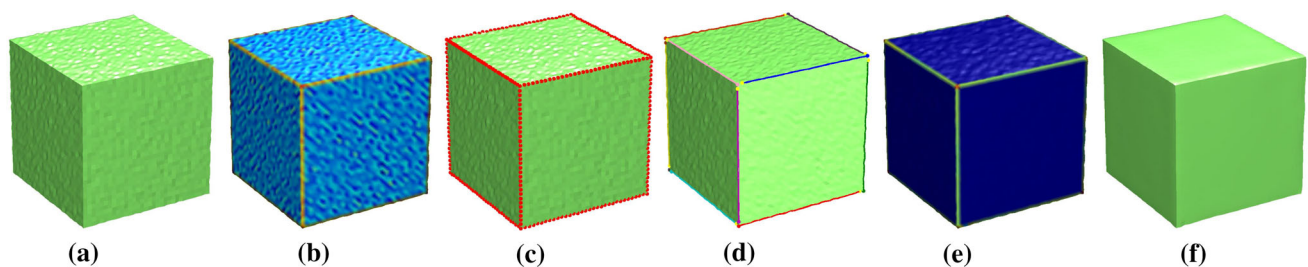


Fig. 4 The outline of feature-preserved surface processing. **a** Original noisy cube model corrupted by 5% Gaussian noise of average lengths of mesh edges. **b** Input signal defined by the mean curvature. **c** Detected

sharp features shown in red color. **d** Connected feature lines shown in different colors. **e** Output signal after our denoising algorithm. **f** Reconstructed model from processed signal

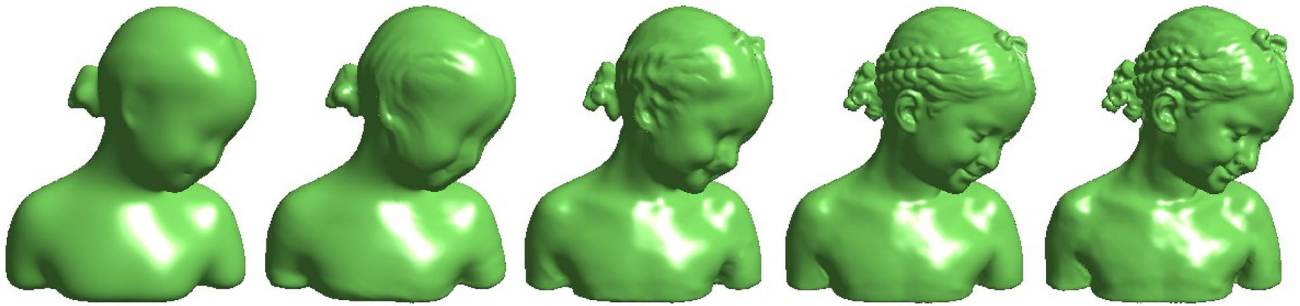


Fig. 5 Filtering results of a Bimba model. From left to right are results of smoothing to enhancing

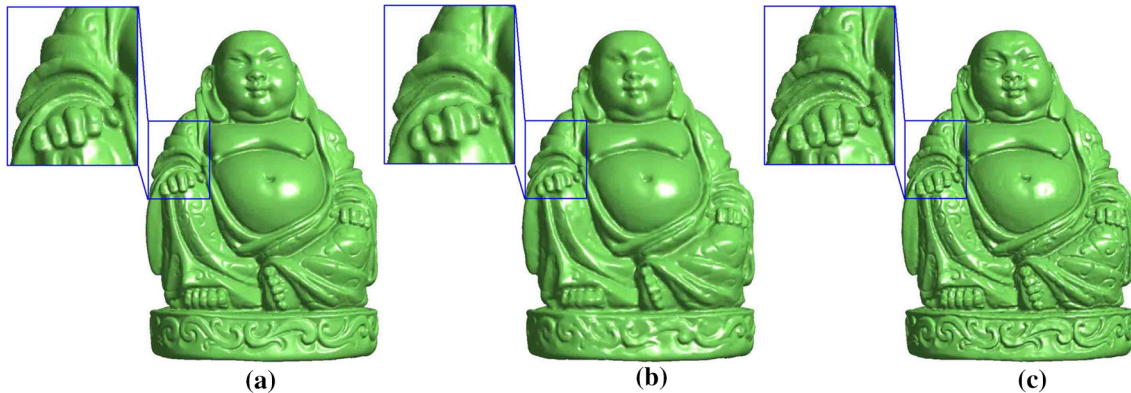


Fig. 6 Smoothing and enhancing results of Buddha model. **a** Original model. **b** Smoothing result by low-pass filter. **c** Enhancing result by high-pass filter

filtered. The advantage of our algorithm can also be verified from the reconstructed result of Fig. 4f, where the sharp feature edges and corners are well preserved.

5 Experimental results

We now document our EMD and Hilbert spectra computation based method for 3D surface processing, which includes surface smoothing, detail enhancing, and feature-preserved denoising.

Surface smoothing and details enhancing. Figure 5 shows a series of results from smoothing to enhancing. The left one is reconstructed from the residue, which is much smoother and merely reveals the general outline of the model. As more high-frequency parts are added, the detail features of the model are becoming more and more clear until the reconstruction result approximates the original model. The last one is the enhancing result and the enhancements can be clearly observed from the hair and nose regions.

Benefitting from the dimensionality reduction, our algorithm can also be used to handle the large-sized model with complex geometry details. In Fig. 6, the results of Buddha model with 700,000+ vertices are shown, in which local regions of the hand are zoomed to illustrate the details of smoothing and enhancing filters.

The flexibility of our scheme based on Hilbert spectra is further verified in Fig. 7, in which the texture features of golf ball can be easily separated and enhanced to generate versatile new models by applying different filters. This modeling advantage also benefits from the fact that our EMD is implemented on 1D signal via dimensionality reduction, which enables us to calculate Hilbert spectra directly on 3D surface. Hilbert spectra provide more information and more flexibility than IMFs to be able to generate various new models.

Feature-preserved surface denoising. Our proposed algorithm can also be used for surface denoising, especially for feature-preserved surface denoising.

Figure 8 shows a denoising result of Torus model. There are no features that can be extracted from the model due to smoothness. Therefore, the denoising result can be directly obtained by filtering the high-frequency part without involving feature separations. From Fig. 8b–d, we can see that the noises are effectively removed by our proposed method as well as the method of bilateral filtering [7] and the Non-Local means based method [32].

For sharp-feature-preserved denoising, we compare our algorithm with the bilateral filtering [7], two-step smoothing [4], original EMD on 3D surface [26] and the EMD-based method with feature constraints [12]. From Fig. 9, we can see that the original EMD could not preserve features and two-step smoothing [4] produces curved edges. With the

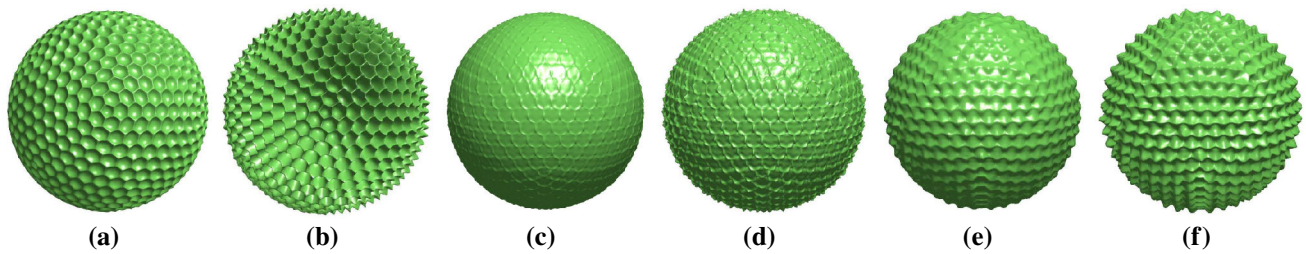


Fig. 7 Various results of a golf ball after applying different filtering. **a–f** Results of high-pass, band-pass, band-stop enhancing filters with increasing enhancing weights, respectively

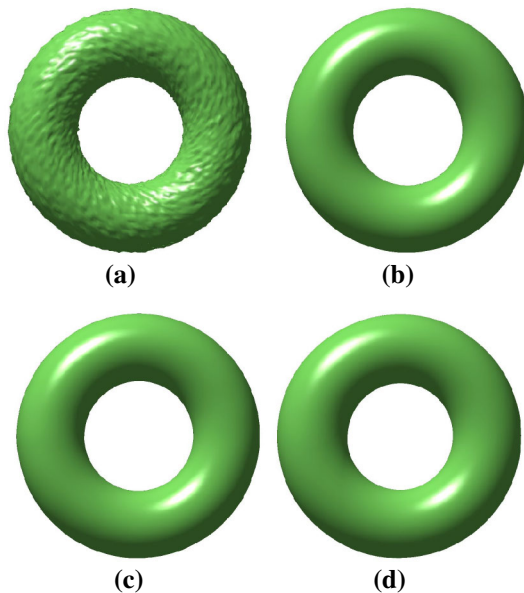


Fig. 8 Denoising result of Torus. **a** Noisy model corrupted by 10% Gaussian noise of average lengths of mesh edges. **b** Results of bilateral filtering [7] after being performed five times with parameters $\sigma_c = 0.4l$ and $\sigma_s = 0.15l$, where l is the average length of mesh edges. **c** Result of Non-Local means based method [32] with $\eta_1 = 3l$, $\eta_2 = 1.3l$ and $\eta_3 = 1.0l$, respectively. **d** Denoising result obtained by our algorithm

feature constraints, the sharp features are well preserved in results of our method as well as the method of [12]. Yet, the method of [12] applies EMD on 3D surface directly, while

our algorithm is implemented on 1D signal, which is much faster.

In Fig. 10, the well-known Fandisk model is further used to illustrate the effectiveness of our algorithm. The model is seriously smoothed by the original EMD. The bilateral filtering [7] can preserve the sharp features well except some weak features on the top fan region. Figure 10d is the result obtained using the method of [12], which can preserve sharp features, but there are still some artifacts occurring on smooth regions. In contrast, with the explicitly feature lines being extracted and the Hilbert spectra guided filtering scheme, our method obtains more satisfactory denoising results with sharp features being fully preserved (see Fig. 10e).

Parameters and timing. In our algorithm, all important parameters are discussed in corresponding sections, such as the stopping criteria of sifting and EMD process, original vertex-constraining weights in surface reconstruction. These parameters are tested in a large number of datasets using default values, which usually lead to satisfactory results.

We have tested our method on numerous models with various sizes. The timings are reported in Table 1, and the implementation is done in MATLAB on a desktop with Inter Core(TM) i7-3770 CPU @3.40GHz 3.90 GHz and 8.0 GB RAM. To obtain the same number of IMFs, our EMD on 1D signal and the entire algorithm are both faster than the EMD on 3D surface, which can be evidently seen from Table 1. For the small-sized Fandisk model in Fig. 10, our 1D EMD is 7 times faster than 3D EMD on surface, while for the large-

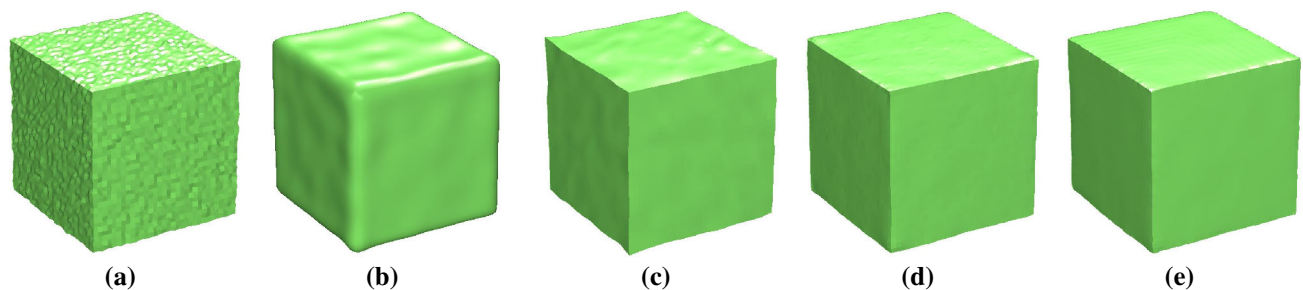


Fig. 9 Feature-preserved denoising results of cube model. **a** Noisy cube corrupted by 10% Gaussian noise of average lengths of mesh edges. **b** Result of original EMD [26] using the 3-th residue. **c** Result of two-step smoothing [4] obtained by MeshLab with 2 smoothing steps,

feature angle threshold 60° , 20 normal smoothing steps and 20 vertex fitting steps. **d** Result of the method [12] using the 3-th residue. **e** Result of our method

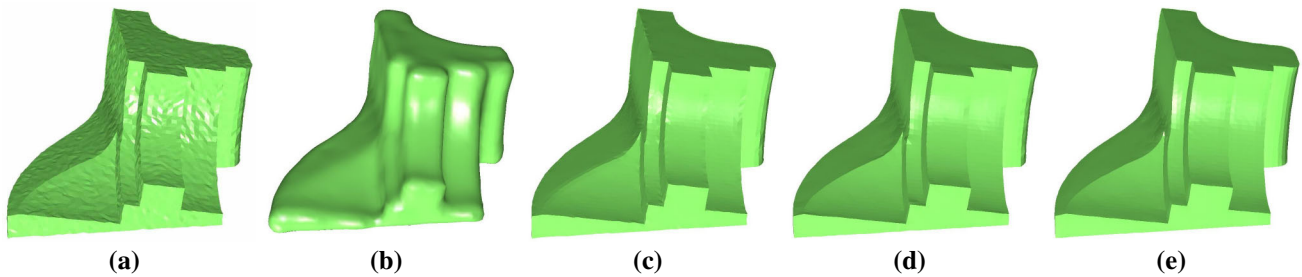


Fig. 10 Feature-preserved denoising result of Fandisk model. **a** The noisy model corrupted by 5% Gaussian noise of average lengths of mesh edges. **b** Result of original EMD on 3D surface [26] using the 3-th residue. **c** Results of bilateral filtering [7] after being performed

three times with parameters $\sigma_c = 0.4l$ and $\sigma_s = 0.05l$, respectively. **d** Reconstructed result using the 3-th residue of the method [12]. **e** Result of our method

Table 1 Run times (in s)

Figs.	#V	#IMF	#IV	3D-EMD	Total	1D-EMD
Fig. 9	6146	12	3	2.63	0.39	1.56
Fig. 10	6475	11	3	2.96	0.42	2.17
Fig. 5	74, 764	13	5	28.14	2.82	4.50
Fig. 7	122, 882	13	3	101.20	4.59	7.13
Fig. 1	134, 345	10	5	96.97	0.74	1.13
Fig. 6	719, 560	15	5	697.89	33.92	60.93

#V: number of vertices. #IMF: number of IMFs. #IV: number of isolated vertices. 3D-EMD: time of EMD directly applied on the signal of 3D surface. 1D-EMD: time of EMD on the 1D signal after dimensionality reduction. Total: total time of our method

sized Hygeia model in Fig. 1, the speedup is more than 100 times.

Discussion During Hamiltonian cycle construction, the input triangular mesh should be a connected manifold without boundaries. The reason is that there is no opposite corner for one corner of the face with boundary in the Corner Table data structure, which is used in the process of Hamiltonian cycle generation [9]. Therefore, if the input mesh has holes or boundaries, it needs to be converted to a closed manifold by any hole-filling algorithms [30,35] or simply building a fan of dummy triangles by connecting the added dummy vertices with boundary vertices.

Limitations. In feature-preserved surface processing, the sharp features should be extracted first. If the models are contaminated by heavy noises, it is difficult to extract the features completely, which will give rise to to-be-blurred features. Another limitation is that the original topology of the mesh connectivity can not be fully preserved in Hamiltonian cycle, which may further result in artefact or feature blurring in case of sharp features not being detected completely. In the near future, we plan to overcome the above limitations by extracting more valuable information from Hilbert spectra to achieve the feature-preserved surface processing in a more automatic manner without human intervention. More broader applications shall be explored based on Hilbert spec-

tra analysis, such as mesh segmentation, shape retrieval, and shape correspondence.

6 Conclusion

In this paper, we have presented a novel EMD and Hilbert spectra computation scheme for 3D geometry analysis and processing via space-filling curve. Based on the exciting idea of dimensionality reduction, the problem of 3D EMD based surface processing is converted to 1D EMD signal processing, which leads to two salient advantages of our algorithm. First, this conversion enables us to calculate Hilbert spectra directly on 3D surface. The newly-obtained Hilbert spectra contain much more quantitative and meaningful information than what IMFs could offer, which can be immediately employed to guide surface processing in a more steerable and precise way to generate versatile results. Second, the high computational cost of EMD on 3D surface processing is significantly reduced by resorting to the dimensionality reduction via Hamiltonian cycle, which can be easily generated on irregular, curved, and complex 3D surfaces. In addition, to overcome the feature blurring limitation of the original EMD and preserve sharp features during 3D surface processing, we have proposed an effective divide-and-conquer EMD decomposition scheme aided by available sharp feature detection techniques. These advantages make our proposed EMD and Hilbert spectra computation based algorithm simple, hence easy to implement on 3D surfaces directly, which have been effectively verified by a large number of experiments.

Acknowledgments We are thankful to Dr. Topraj Gurung and Dr. Mark Luffel for discussing and providing the code of Hamilton cycle generation. This work is supported in part by National Science Foundation of USA (IIS-0949467, IIS-1047715, and IIS-1049448), National Natural Science Foundation of China (No. 61190120, 61190121, 61190125, 61202261), China Postdoctoral Science Foundation (No. 2014M560875), Scientific and Technological Development Plan of Jilin Province (No. 20130522113JH). Models are courtesy of AIM@SHAPE Repository.

References

- Akleman, E., Xing, Q., Garigipati, P., Taubin, G., Chen, J., Hu, S.: Hamiltonian cycle art: surface covering wire sculptures and duotone surfaces. *Comput. Graph.* **37**(5), 316–332 (2013)
- Ali, H., Hariharan, M., Yaacob, S., Adom, A.H.: Facial emotion recognition using empirical mode decomposition. *Expert Syst. Appl.* **42**(3), 1261–1277 (2015)
- Arkin, E., Held, M., Mitchell, J., Skiena, S.: Hamiltonian triangulations for fast rendering. *Vis. Comput.* **12**(9), 429–444 (1996)
- Belyaev, A., Ohtake, Y.: A comparison of mesh smoothing methods. In: Israel-Korea bi-national conference on geometric modeling and computer graphics, pp. 83–87 (2003)
- Coifman, R.R., Maggioni, M.: Diffusion wavelets. *Appl. Comput. Harmon. Anal.* **21**(1), 53–94 (2006)
- Di, C., Yang, X., Wang, X.: A four-stage hybrid model for hydrological time series forecasting. *PLoS ONE* **9**(8), e104–663 (2014)
- Fleishman, S., Drori, I., Cohen-Or, D.: Bilateral mesh denoising. *ACM Trans. Graph.* **22**(3), 950–953 (2003)
- Gao, Y., Li, C.F., Ren, B., Hu, S.M.: View-dependent multiscale fluid simulation. *IEEE Trans. Vis. Comput. Graph.* **19**(2), 178–188 (2013)
- Gurung, T., Luffel, M., Lindstrom, P., Rossignac, J.: Lr: compact connectivity representation for triangle meshes. *ACM Trans. Graph.* **30**(4), 67:1–67:8 (2011)
- Guskov, I., Sweldens, W., Schröder, P.: Multiresolution signal processing for meshes. In: *SIGGRAPH'99*, pp. 325–334 (1999)
- Hou, T., Qin, H.: Admissible diffusion wavelets and their applications in space-frequency processing. *IEEE Trans. Vis. Comput. Graph.* **19**(1), 3–15 (2013)
- Hu, J., Wang, X., Qin, H.: Improved, feature-centric emd for 3d surface modeling and processing. *Graph. Models* **76**(5), 340–354 (2014)
- Huang, N.E., Shen, Z., Long, S.R., Wu, M.C., Shih, H.H., Zheng, Q., Yen, N.C., Tung, C.C., Liu, H.H.: The empirical mode decomposition and the hilbert spectrum for nonlinear and non-stationary time series analysis. *Proc. R. Soc. Lond. A* **454**(1971), 903–995 (1998)
- Jones, T.R., Durand, F., Desbrun, M.: Non-iterative, feature-preserving mesh smoothing. *ACM Trans. Graph.* **22**(3), 943–949 (2003)
- Kopsinis, Y., McLaughlin, S.: Development of emd-based denoising methods inspired by wavelet thresholding. *IEEE Trans. Signal Process.* **57**(4), 1351–1362 (2009)
- Mandic, D., Rehman, N., Wu, Z., Huang, N.: Empirical mode decomposition-based time-frequency analysis of multivariate signals: the power of adaptive data analysis. *IEEE Signal Process. Mag.* **30**(6), 74–86 (2013)
- Peano, G.: Sur une courbe, qui remplit toute une aire plane. *Mat. Ann.* **36**(1), 157–160 (1890)
- Qin, X., Hong, C.X., Zhang, S.Q., Wang, W.H.: Emd based fairing algorithm for mesh surface. In: *CAD/Graphics '09*, pp. 606–609 (2009)
- Quinn, J., Langbein, F., Lai, Y.K., Martin, R.: Generalized anisotropic stratified surface sampling. *IEEE Trans. Vis. Comput. Graph.* **19**(7), 1143–1157 (2013)
- Ren, B., Li, C.F., Lin, M., Kim, T., Hu, S.M.: Flow field modulation. *IEEE Trans. Vis. Comput. Graph.* **19**(10), 1708–1719 (2013)
- Schröder, P., Sweldens, W.: Spherical wavelets: efficiently representing functions on the sphere. In: *SIGGRAPH '95*, pp. 161–172 (1995)
- Solomon, J., Crane, K., Butscher, A., Wojtan, C.: A general framework for bilateral and mean shift filtering. *CoRR abs/1405.4734* (2014)
- Subr, K., Soler, C., Durand, F.: Edge-preserving multiscale image decomposition based on local extrema. *ACM Trans. Graph.* **28**(5), 147:1–147:9 (2009)
- Taubin, G.: A signal processing approach to fair surface design. In: *SIGGRAPH*, pp. 351–358 (1995)
- Taubin, G.: Constructing hamiltonian triangle strips on quadrilateral meshes. In: *Visualization and Mathematics III, Mathematics and Visualization*, pp. 69–91 (2003)
- Wang, H., Su, Z., Cao, J., Wang, Y., Zhang, H.: Empirical mode decomposition on surfaces. *Graph. Models* **74**(4), 173–183 (2012)
- Wang, R., Yang, Z., Liu, L., Deng, J., Chen, F.: Decoupling noises and features via weighted l1-analysis compressed sensing. *ACM Trans. Graph.* **33**(2), 18:1–18:12 (2014)
- Wang, S., Hou, T., Su, Z., Qin, H.: Multi-scale anisotropic heat diffusion based on normal-driven shape representation. *Vis. Comput.* **27**(6–8), 429–439 (2011)
- Wang, X., Cao, J., Liu, X., Li, B., Shi, X., Sun, Y.: Feature detection of triangular meshes via neighbor supporting. *J. Zhejiang Univ. Sci. C* **13**(6), 440–451 (2012)
- Wang, X., Liu, X., Lu, L., Li, B., Cao, J., Yin, B., Shi, X.: Automatic hole-filling of cad models with feature-preserving. *Comput. Graph.* **36**(2), 101–110 (2012)
- Wu, Z., Huang, N.E., Chen, X.: The multi-dimensional ensemble empirical mode decomposition method. *Adv. Adapt. Data Anal.* **01**(03), 339–372 (2009)
- Yoshizawa, S., Belyaev, A., peter Seidel, H.: Smoothing by example: mesh denoising by averaging with similarity based weights. In: *Proceedings of the IEEE international conference on shape modeling and applications* (2006), pp. 38–44. *IEEE* (2006)
- Zang, Y., Huang, H., Zhang, L.: Efficient structure-aware image smoothing by local extrema on space-filling curve. *IEEE Trans. Vis. Comput. Graph.* **20**(9), 1253–1265 (2014)
- Zhang, J., Zheng, C., Hu, X.: Triangle mesh compression along the hamiltonian cycle. *Vis. Comput.* **29**(6–8), 717–727 (2013)
- Zhao, W., Gao, S., Lin, H.: A robust hole-filling algorithm for triangular mesh. *Vis. Comput.* **23**(12), 987–997 (2007)
- Zhong, M., Qin, H.: Sparse approximation of 3d shapes via spectral graph wavelets. *Vis. Comput.* **30**(6–8), 751–761 (2014)



Xiaochao Wang is a postdoctoral in the school of computer science and engineering at Beihang University. He received his Ph.D degree in Computational Mathematics from Dalian University of Technology in 2014. His research interests include mesh and point clouds processing.



Jianping Hu is an associate professor in College of Science at Northeast Dianli University. He obtained his B.S and M.S in Mathematics at Jilin University. He received his Ph.D in Computational Mathematics from Dalian University of Technology in 2009. His research interests include computational geometry, computer graphics, and image processing and analysis.



Hong Qin is a full professor of Computer Science in Department of Computer Science at Stony Brook University (SUNY). He received his B.S. and his M.S. in Computer Science from Peking University, China. He received his Ph.D. in Computer Science from the University of Toronto. Currently, he serves as an associate editor for *The Visual Computer*, *Graphical Models*, and *Journal of Computer Science and Technology*.

His research interests include geometric and solid modeling, graphics, physics-based modeling and simulation, computer aided geometric design, human-computer interaction, visualization, and scientific computing.



Dongbo Zhang is a Ph.D student in the school of computer science and engineering at Beihang University. He received his B.S in Xidian University in 2014. His research interests include mesh and point clouds processing.